Journal of Organometallic Chemistry 751 (2014) 686–694

Contents lists available at ScienceDirect

Journal of Organometallic Chemistry

journal homepage: www.elsevier.com/locate/jorganchem

Synthesis of a 14-electron iridium(III) complex with a xanthene-based bis(silyl) chelate ligand (xantsil): A distorted seesaw-shaped four-coordinate geometry and reactions leading to 16-electron complexes

Takashi Komuro, Keisuke Furuyama, Takeo Kitano, Hiromi Tobita*

Department of Chemistry, Graduate School of Science, Tohoku University, Sendai 980-8578, Japan

ARTICLE INFO

Article history:
Received 11 August 2013
Received in revised form
5 September 2013
Accepted 6 September 2013

Keywords:
Iridium
14-Electron complex
Bis(silyl) chelate ligand
Xanthene-based ligand
Seesaw-shaped complex
Alkene hydrogenation

ABSTRACT

Synthesis, structure determination, and reactions of a 14-electron four-coordinate iridium(III) complex bearing a xanthene-based bis(silyl) chelate ligand, i.e., Ir{κ^2(*Si*,*Si*)-xantsil}(PCy_3)Cl (**1a**, xantsil = (9,9-dimethylxanthene-4,5-diyl)bis(dimethylsilyl)), are reported. A precursor of **1a**, the 16-electron (dihydrido)iridium(V) complex Ir{κ^2(*Si*,*Si*)-xantsil}$(H)_2$(PCy_3)Cl (**2**), was prepared by the reaction of $[IrCl\text{-}(coe)_2]_2$ (coe = cyclooctene) with 4,5-bis(dimethylsilyl)-9,9-dimethylxanthene (xantsilH_2) and PCy_3. Dehydrogenation reaction of **2** with 3,3-dimethylbut-1-ene, a hydrogen acceptor, afforded a mixture of **1a** and its isomer **1b**, abbreviated as **1a** + **1b**, together with 2,2-dimethylbutane. Single crystals obtained from a CH_2Cl_2 solution of **1a** + **1b** contained only isomer **1a**. X-ray crystal structure analysis of one of the crystals revealed that **1a** adopts a distorted seesaw-shaped four-coordinate geometry where the coordinatively unsaturated metal center is stabilized by weak agostic interaction of two γ-C–H bonds of the PCy_3 ligand. On the other hand, NMR spectroscopic analysis of **1a** + **1b** demonstrated that **1a** is in fast equilibrium with a minor amount of **1b** in solution. Replacement of the chloro ligand in complexes **1a** + **1b** by a triflato ligand with AgOTf (OTf = OSO_2CF_3) afforded quantitatively a single product, i.e., the 16-electron iridium–triflato complex Ir{κ^3(*Si*,*O*,*Si*)-xantsil}(PCy_3)(OTf) (**3**). **1a** + **1b** and 16-electron complex **2** are interconvertible via oxidative addition of dihydrogen (from **1a** + **1b** to **2**) and alkene hydrogenation (from **2** to **1a** + **1b**). Complexes **1a** + **1b** and **2** were found to catalyze hydrogenation of 3,3-dimethylbut-1-ene.

1. Introduction

Transition-metal complexes bearing silyl-containing multidentate chelate ligands are increasingly attracting considerable attention due to their unique properties (molecular structures and reactivity) and potential applications as catalysts [1]. These complexes containing normally labile silyl ligands are stabilized by the chelate-effect of the multidentate ligand. One of the characteristic features of these complexes is the ability to generate and stabilize reactive species with a coordinatively unsaturated metal center in which the vacant coordination sites are in most cases located *trans* to the silyl coordination sites. This feature is attributable to the following properties of the silyl coordination sites in the multidentate ligands: (1) Strong σ-donating ability of the silyl ligand that makes the metal center electron rich and compensates the electronic unsaturation of the metal center [2], and (2) strong *trans* influence of the silyl ligand that weakens the coordinate bonds *trans* to the silyl coordination sites [3]. For instance, Turculet et al. have recently succeeded in isolation and structural determination of four-coordinate 14-electron Ru complexes having a tridentate PSiP ligand [4]. These complexes adopt an unusual trigonal pyramidal geometry where the silyl moiety of the PSiP ligand occupies the apical position. It is proposed that this geometry is enforced by the strong σ-donating silyl coordination site in the PSiP ligand.

In this context, we have developed a xanthene-based bis(silyl) chelate ligand "xantsil" ((9,9-dimethylxanthene-4,5-diyl)bis(dimethylsilyl)) as a supporting ligand effective for stabilizing coordinatively unsaturated complexes [5]. The xantsil ligand having double silyl coordination sites is considered to stabilize and generate reactive, coordinatively unsaturated species more efficiently than the multidentate ligands having only a single silyl coordination site. Moreover, the xantsil ligand functions as a hemilabile ligand because the ether-oxygen atom in the xanthene backbone can weakly coordinate to a metal center. Thus, both κ^2(*Si*,*Si*) and κ^3(*Si*,*O*,*Si*) coordination modes are possible (Scheme 1),

* Corresponding author. Tel.: +81 22 795 6539; fax: +81 22 795 6543.
E-mail address: tobita@m.tohoku.ac.jp (H. Tobita).

0022-328X/$ – see front matter © 2013 Elsevier B.V. All rights reserved.
http://dx.doi.org/10.1016/j.jorganchem.2013.09.009

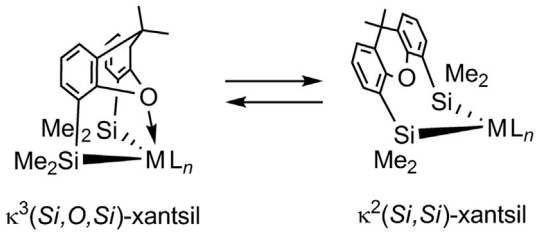

Scheme 1. Hemilability of the xantsil ligand.

and facile dissociation of the coordinated oxygen in $\kappa^3(Si,O,Si)$-xantsil complexes generates coordinatively unsaturated $\kappa^2(Si,Si)$-xantsil complexes under mild conditions [5].

In our research on the chemistry of metal–xantsil complexes, we have focused on attempting to synthesize the iridium–xantsil complexes. This is because iridium is known to form stable metal–silyl complexes in various oxidation states, which are potentially highly active as catalysts [1,6,7]. In this study, we succeeded in the synthesis of a 14-electron ($\kappa^2(Si,Si)$-xantsil)iridium complex with a unique distorted seesaw-shaped four-coordinate geometry. We also found that the 14-electron complex exists as an equilibrium mixture with an isomeric 16-electron $\kappa^3(Si,O,Si)$-xantsil complex (a putative structure) and that the equilibrium mixture is an active catalyst for alkene hydrogenation.

2. Results and discussion

2.1. Synthesis of 16-electron iridium–xantsil complex 2

(Dihydrido)iridium(V) complex Ir{$\kappa^2(Si,Si)$-xantsil}$(H)_2(PCy_3)Cl$ (**2**), a precursor of the synthetic target Ir{$\kappa^2(Si,Si)$-xantsil}$(PCy_3)Cl$ (**1a**), was prepared in 68% yield by the reaction of a dinuclear iridium(I) complex $[IrCl(coe)_2]_2$ (coe = cyclooctene) with 4,5-bis(dimethylsilyl)-9,9-dimethylxanthene ($xantsilH_2$) [5a,b] and PCy_3 (1:2.1:2.7 M ratio, simultaneous mixing) in toluene at room temperature (Scheme 2). Oxidative addition of two Si–H bonds of $xantsilH_2$ and substitution of PCy_3 for coe took place at the iridium center. Importantly, the main product(s) of this reaction changed by changing the order of the addition of $xantsilH_2$ and PCy_3. Thus, in contrast with the above procedure producing **2**, addition of $xantsilH_2$ and then PCy_3 to $[IrCl(coe)_2]_2$ in toluene resulted in direct formation of a mixture of **1a** and its isomer **1b** in 48% isolated yield together with cyclooctane (Scheme 3, also see 2.3). This result implies that, in the former reaction producing **2**, $[IrCl(coe)_2]_2$ reacts first with PCy_3 and then with $xantsilH_2$. In fact, the NMR-tube reaction of $[IrCl(coe)_2]_2$ with PCy_3 (3 equiv) and then $xantsilH_2$ (2 equiv) in C_6D_6 at room temperature predominantly afforded complex **2**.

2.2. Characterization of complex 2

Single crystal X-ray analysis revealed that **2** has a chloro, PCy_3, and xantsil ligands and they adopt a distorted pseudo-tetrahedral geometry (Fig. 1). The bond angles around the metal center range widely from 91.74(6)° to 125.49(7)°. The Ir–Si bond distances (Ir–Si1 = 2.372(2), Ir–Si2 = 2.344(2) Å) are rather normal for typical (silyl)iridium complexes (2.235(5)–2.479(2) Å) [8]. Although the hydrido ligands of **2** could not be located in the final difference Fourier map, the following spectroscopic features support the existence of two hydrido ligands on iridium: The ^1H NMR spectrum of **2** at room temperature in C_6D_6 shows two broad signals assigned to the hydrido ligands at −14.33 and −5.34 ppm in the same intensity. The IR spectrum of **2** also exhibits two absorption bands at 2297 and 2173 cm^{-1} attributable to the two stretching modes of the H–Ir–H linkage.

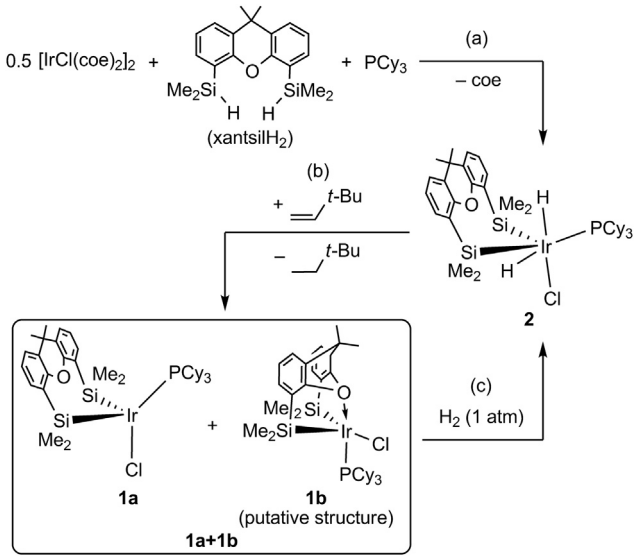

Scheme 2. Synthesis of iridium–xantsil complexes **1a** + **1b** and **2** and interconversion pathways between them. Reaction conditions: (a) simultaneous mixing of the reagents, toluene, r.t., 1 h; (b) toluene, 60 °C, 30 h; (c) C_6D_6, r.t., 24 h.

The positions of the hydrido ligands can be estimated by comparing the bond angles around the metal center in **2**. The Cl–Ir–Si1 (125.49(7)°) and P–Ir–Si1 (122.22(7)°) angles are considerably wider than other bond angles, while the Cl–Ir–P (91.74(6)°) angle is the narrowest. Thus, the two hydrido ligands are considered to be located in the area surrounded by the P, Si1, and Si2 atoms and that surrounded by the Cl, Si1, and Si2 atoms. This indicates that complex **2** adopts a bicapped-tetrahedral geometry in which the *trans* arrangements of strongly σ-donating ligands, i.e., silyl–hydrido and hydrido–hydrido, are avoided. Similar bicapped-tetrahedral geometries have been reported by Tilley et al. for bis-(silyl)(dihydrido)iridium(V) complexes possessing a pyridylindolide or a pyridyl-pyrrolide chelate ligand [9].

The observation of two broadened ^1H NMR signals for the hydrido ligands in **2** implies the existence of a dynamic behavior exchanging the two hydrido ligands in solution. This was confirmed by variable-temperature ^1H NMR spectroscopy (see Fig. B1 in the Supplementary material): When a solution of **2** in toluene-d_8 was cooled to 243 K, the hydrido signals appeared as two sharp doublets

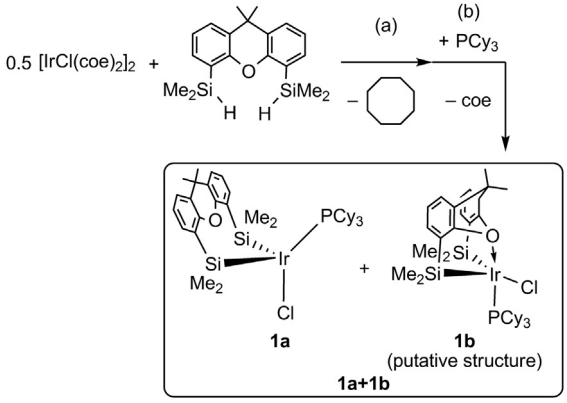

Scheme 3. One-pot synthesis of **1a** + **1b** from $[IrCl(coe)_2]_2$. Reaction conditions: (a) toluene, r.t., 30 min, (b) toluene, r.t., 30 min.

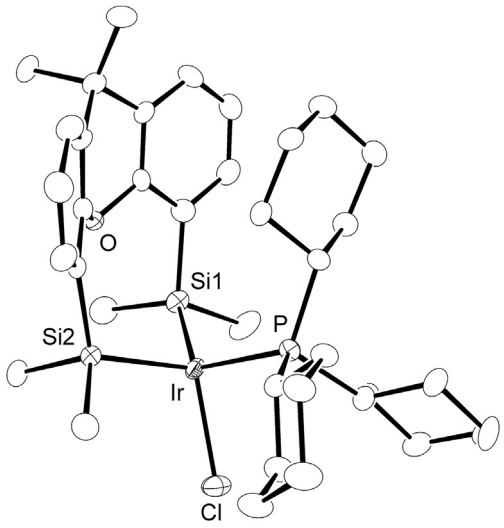

Fig. 1. Molecular structure of Ir{κ²(*Si*,*Si*)-xantsil}(H)₂(PCy₃)Cl (**2**) (50% probability ellipsoids). Hydrogen atoms are omitted for clarity. Selected bond distances (Å) and angles (°) for **2**: Ir–Cl 2.3771(18), Ir–P 2.4014(18), Ir–Si1 2.372(2), Ir–Si2 2.344(2); Cl–Ir–P 91.74(6), Cl–Ir–Si1 125.49(7), Cl–Ir–Si2 105.88(7), P–Ir–Si1 122.22(7), P–Ir–Si2 108.94(7), Si1–Ir–Si2 101.44(7).

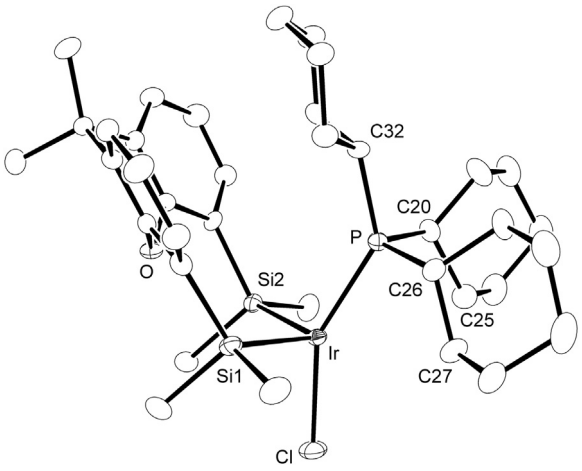

Fig. 2. Molecular structure of Ir{κ²(*Si*,*Si*)-xantsil}(PCy₃)Cl (**1a**) (50% probability ellipsoids). Hydrogen atoms are omitted for clarity. Selected interatomic distances (Å) and angles (°) for **1a**: Ir–Cl 2.3157(11), Ir–P 2.2593(11), Ir–Si1 2.3316(13), Ir–Si2 2.3229(12), Ir···C25 3.390(5), Ir···C27 3.192(5); Cl–Ir–P 150.64(4), Cl–Ir–Si1 95.37(5), Cl–Ir–Si2 94.01(4), P–Ir–Si1 104.08(4), P–Ir–Si2 103.64(4), Si1–Ir–Si2 100.47(4), Ir–P–C20 103.56(15), Ir–P–C26 101.89(16), Ir–P–C32 136.76(15).

at −14.16 ($^2J_{PH}$ = 22 Hz) and −5.07 ($^2J_{PH}$ = 112 Hz) ppm coupled with the phosphorus of the PCy_3 ligand. These signals broadened at room temperature and became much broader at higher temperatures. Existence of the process exchanging the two hydrido ligands was further supported by the measurement of the 2D EXSY NMR spectrum [10] for **2** at 243 K where the EXSY cross peaks were observed between the hydrido signals (see Fig. B2 in the Supplementary material).

The coupling constants between the hydrogen and phosphorus nuclei observed in the ^{1}H NMR signals of the hydrido ligands at 243 K are consistent with the positions of the hydrido ligands estimated by the single crystal X-ray analysis (vide supra). Thus, the large coupling constant ($^2J_{PH}$ = 112 Hz) for the signal at −5.07 ppm indicates that the hydrogen atom is approximately *trans* to phosphorus, whereas the small coupling constant ($^2J_{PH}$ = 22 Hz) for the signal at −14.16 ppm indicates that the hydrogen atom is located at a position nearly *cis* to phosphorus. Similar $^2J_{PH}$ values, i.e., 117 (*trans* to phosphorus) and 18 (*cis* to phosphorus) Hz, have been reported for one of the hydrido signals of bis(silyl)(trihydrido)iridium(V) complex Ir{*o*-$(Me_2Si)_2C_6H_4$}$(H)_3(PPh_3)_2$ [7b].

The spin-lattice relaxation times (T_1) of the two hydrido ligands of **2** were determined using the inversion-recovery method by ^{1}H NMR spectroscopy. The values at 183 K for the signals at −13.98 and −4.69 ppm are 2.3 s and 1.8 s, respectively. These T_1 values are typical of dihydrido complexes (T_1 > 150 ms) [11]. Thus, complex **2** is regarded not as an η^2-dihydrogen complex but as a dihydrido complex.

The ^{29}Si{^{1}H} NMR spectrum of **2** shows a singlet at −1.6 ppm, indicating that the two silicon nuclei in the xantsil ligand are equivalent in solution. This chemical shift is close to that (1.05 ppm) for a bis(silyl)(dihydrido)iridium(V) complex (η^5-C_5Me_5)Ir{*o*-$(Me_2Si)_2C_6H_4$}$(H)_2$ [7c]. The observation of the ^{29}Si NMR signal of **2** as a singlet implies that the coupling with the phosphorus nucleus is negligible.

2.3. Synthesis of 14-electron iridium–xantsil complex *1a* and its isomer *1b*

Ir{κ²(*Si*,*Si*)-xantsil}(H)₂(PCy₃)Cl (**2**) reacted with 3,3-dimethylbut-1-ene, a hydrogen acceptor [12], at 60 °C in toluene to give a dehydrogenation product Ir(xantsil)(PCy₃)Cl as a mixture of isomers **1a** and **1b**, together with 2,2-dimethylbutane (Scheme 2). The product was isolated from the reaction mixture as a reddish orange powder in 45% yield. As will be described in sections 2.4–2.6, the product exists as an equilibrium mixture of two isomers **1a** (major) and **1b** (minor) in solution, but exists as only **1a** in the solid state. The same reaction was carried out in C_6D_6 and was monitored by ^{1}H NMR spectroscopy, which revealed that 2,2-dimethylbutane was formed in parallel with the formation of **1a** + **1b**. 2,2-Dimethylbutane in the reaction mixture was identified by comparison of its ^{1}H and ^{13}C{^{1}H} NMR spectra and GC retention time with those of its authentic sample.

The same product **1a** + **1b** was also formed mainly and was isolated in 48% yield by the reaction of $[IrCl(coe)_2]_2$ with xantsilH_2 (2.3 equiv) in toluene at room temperature followed by the reaction with PCy_3 (2.3 equiv) in one-pot (Scheme 3). The same reaction conducted in an NMR tube using C_6D_6 as a solvent ($[IrCl(coe)_2]_2$:xantsilH_2:PCy_3 = 1:2:3 in molar ratio) revealed that cyclooctane was formed as a main product together with **1a** + **1b**, which were identified by ^{1}H, ^{13}C{^{1}H}, and ^{31}P{^{1}H} NMR spectroscopy in the reaction mixture. This observation clearly shows that some of the cyclooctene ligands in $[IrCl(coe)_2]_2$ were hydrogenated in this reaction.

2.4. Crystal structure analysis of 14-electron complex *1a*

Recrystallization of **1a** + **1b** from CH_2Cl_2 afforded reddish orange crystals, from which one crystal was selected and analyzed by X-ray diffraction method. As a result, the crystal was found to be a single crystal of **1a** and the molecular structure was determined unequivocally (Fig. 2). Complex **1a** has a four-coordinate structure composed of a bidentate xantsil, PCy_3, and chloro ligands, and their arrangement is considerably distorted from the ideal tetrahedral geometry. The Cl–Ir–P angle (150.64(4)°) is much wider than other bond angles around the metal center in **1a** (94.01(4)–104.08(4)°) and also the Cl–Ir–P angle in **2** (91.74(6)°). The molecular structure of **1a** can be best described as a distorted seesaw-shaped geometry where the Cl–Ir–P moiety corresponds to the long board of the seesaw [13]. The Ir–Cl, Ir–P, and Ir–Si bond distances (2.3157(11), 2.2593(11), and av. 2.3273(18) Å, respectively) are all slightly shortened in comparison with the corresponding distances of **2**

(2.3771(18), 2.4014(18), and av. 2.358(3) Å, respectively), which is attributable to the decrease of the coordination number of **1a** in comparison with that of **2**.

The coordinatively unsaturated iridium center in **1a** is considered to be stabilized by weak agostic interaction of two C–H bonds directed toward the vacant coordination sites located in the widened Cl–Ir–P bond angle. Two methylene moieties (C25 and C27) in two cyclohexyl groups are located *trans* to the silyl ligands and are somewhat close to the metal center: The Ir···C_γ interatomic distances (Ir···C25: 3.390(5) Å, Ir···C27: 3.192(5) Å) are nearly identical with the sum (3.22 Å) of the van der Waals radius of a methylene group (2.0 Å) [14] and a single-bond covalent radius of iridium (1.22 Å) [15]. The existence of weak agostic interaction is also supported by the narrowing of Ir–P–C20 and Ir–P–C26 angles (103.56(15) and 101.89(16)°, respectively) compared with the Ir–P–C32 angles (136.76(15)°) where the former two carbons C20 and C26 belong to the cyclohexyl groups with the weak agostic interaction [16]. Similar weak C–H agostic interaction between a metal and two γ-carbons in a cyclohexyl group of PCy_3 has been found in the 16-electron Ru–xantsil complex Ru{κ^3(*Si*,*O*,*Si*)-xantsil}(P-Cy_3)(CO) [5f].

The two γ-C–H agostic interactions in **1a** are substantially weak as demonstrated by the Ir···C25 and Ir···C27 interatomic distances that are much longer than the Ir···C_γ(cyclohexyl) distance (2.923(10) Å) in the tris(phosphine)iridium complex [$Ir(H)_2(PCy_2Ph)_3$][BAr'_4] (Ar′ = 3,5-$(CF_3)_2C_6H_3$) having a normal agostic interaction between the iridium(III) center and a γ-C–H bond of a cyclohexyl group on phosphorus [16a]. This weakening of the agostic interactions is attributable to the strong *trans*-influence of the silyl ligands Si1 and Si2 located *trans* to C27 and C25, respectively. If we neglect these very weak agostic interactions, **1a** can be regarded as a 14-electron bis(-silyl)iridium(III) complex. To the best of our knowledge, **1a** is the first crystallographically characterized 14-electron bis(silyl)iridium complex and is also a rare example of isolated 14-electron iridium(III) complexes [16,17].

2.5. Spectroscopic characterization of *1a* + *1b*

Although elemental analysis and mass spectroscopic data confirm that the molecular formula of **1a** + **1b** is "Ir(xantsil)(PCy_3)Cl", the NMR spectroscopic analysis of **1a** + **1b** in solution revealed that this compound exists as an equilibrium mixture of two isomeric Ir–xantsil complexes **1a** (major) and **1b** (minor) (see Fig. B3–6 in the Supplementary material). The ^{1}H NMR spectrum of **1a** + **1b** in CD_2Cl_2 shows four sharp SiMe signals at 0.72, 0.85 ppm (**1a**) and 0.36, 0.77 ppm (**1b**) with a *ca.* 5:5:1:1 intensity ratio. In the ^{29}Si{^{1}H} NMR spectrum of **1a** + **1b** in CD_2Cl_2, two doublets were observed at −17.5 (**1a**, $^2J_{SiP}$ = 8.4 Hz) and −6.2 (**1b**, $^2J_{SiP}$ = 9.9 Hz) ppm. These signals are shifted upfield in comparison with that of **2** (−1.6 ppm). The ^{31}P{^{1}H} NMR spectrum of **1a** + **1b** in CD_2Cl_2 exhibits two broad signals for **1a** and **1b** at 0.5 ppm ($\Delta\nu_{1/2}$ = 12 Hz) and 9.1 ppm ($\Delta\nu_{1/2}$ = 8 Hz), respectively. The broadening of these signals is possibly caused by the fast interconversion between **1a** and **1b**. These signals are also substantially shifted upfield in comparison with that for **2** (41.5 ppm).

The molar ratio of **1a** and **1b** in solution changes depending on the solvent, i.e., **1a**:**1b** = 5:1 in CD_2Cl_2 and 8:1 in C_6D_6. This also implies that the fast equilibrium between **1a** and **1b** exists. The 2D EXSY measurement of **1a** + **1b** in CD_2Cl_2 at room temperature clearly demonstrated it (Fig. 3). Two EXSY cross peaks were observed between the SiMe signal of **1a** at 0.72 ppm and that of **1b** at 0.36 ppm and between the SiMe signal of **1a** at 0.85 ppm and that of **1b** at 0.77 ppm. These observations indicate that two sets of exchange between SiMe groups of **1a** and **1b** exist and are caused by the fast equilibrium.

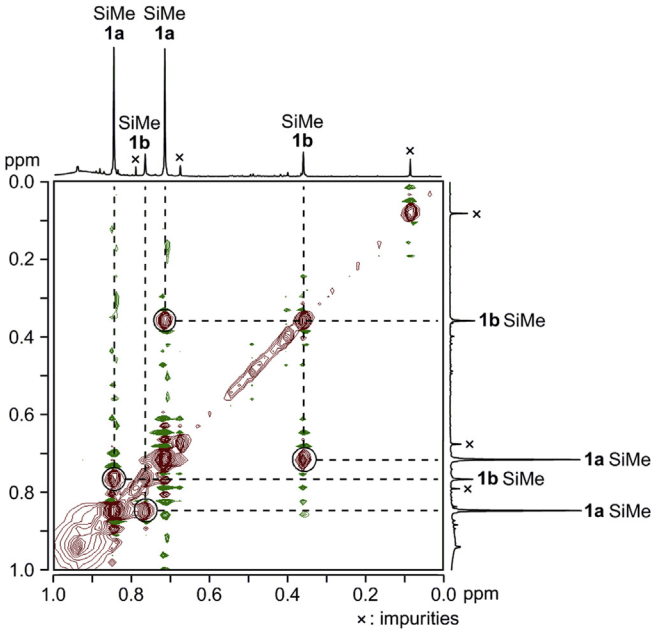

Fig. 3. 2D EXSY NMR spectrum (in the range of 0–1 ppm) of **1a** + **1b** (700 MHz, r.t., CD_2Cl_2).

2.6. Solid state NMR spectroscopic analysis of *1a* + *1b*

To clarify the composition of **1a** and **1b** in the solid state, an NMR spectrum of a solid sample of **1a** + **1b** was measured, which revealed that **1a** existed exclusively in the solid state in accordance with the result of the X-ray crystal structure analysis [18]. The ^{31}P{^{1}H} CPMAS NMR spectrum shows two signals at −2.1 and 1.1 ppm with nearly the same intensity (see Fig. B7 in the Supplementary material). These chemical shifts are close to that of the ^{31}P NMR signal of **1a** in solution (0.5 ppm in CD_2Cl_2, 1.8 ppm in C_6D_6), and there were no signals in the region where **1b** showed its signal in solution (9.1 ppm in CD_2Cl_2, 9.6 ppm in C_6D_6). Therefore, the two ^{31}P signals of the solid sample can be both attributed to **1a**. The observation of two ^{31}P signals implies that the solid sample contains two crystallographically independent molecules of **1a** [19]. This sample was obtained as orange crystals by recrystallization of crude **1a** + **1b** from a THF/hexane solution, but its crystal structure was not determined. The molecular packing in this sample is considered to be different from that in the single crystal of **1a** used for the X-ray analysis (see 2.4) where the asymmetric unit contains only one independent molecule of **1a** together with one molecule of CH_2Cl_2 as the solvent of crystallization.

2.7. Conversion of chloro complexes *1a* + *1b* into triflato complex *3*

Replacement of the chloro ligand on iridium of **1a** and **1b** by a triflato ligand was examined by treatment of **1a** + **1b** with silver trifluoromethanesulfonate (AgOTf) in C_6D_6 at room temperature. This reaction gave a single product Ir{κ^3(*Si*,*O*,*Si*)-xantsil}(PCy_3)(OTf) (**3**) quantitatively (*ca.* 100% NMR yield) (Scheme 4). Both **1a** and **1b** were converted into **3**, and this fact further supports that **1b** is an isomer of **1a**. A preparative scale reaction of **1a** + **1b** with AgOTf in toluene resulted in isolation of **3** in 65% yield after removal of precipitated AgCl.

2.8. Characterization of triflato complex *3*

The molecular structure of **3** was confirmed by single crystal X-ray analysis (Fig. 4): Complex **3** adopts a distorted square pyramidal

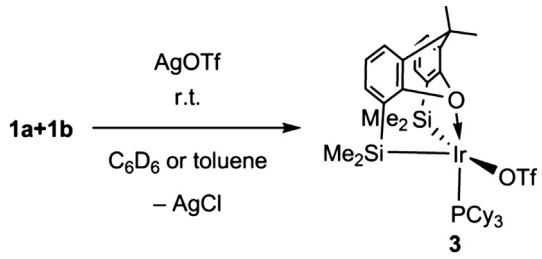

Scheme 4. Reaction of iridium–xantsil complexes **1a** + **1b** with AgOTf that gives a single complex **3**.

geometry composed of a κ^3(*Si*,*O*,*Si*)-xantsil ligand, a PCy_3 ligand, and a triflato ligand. The tridentate xantsil ligand is facially coordinated to iridium. The Ir–O1 distance (2.245(4) Å) is close to the Ir–O(xanthene) distance (2.220(3) Å) in the diiridium complex having a κ^3(*P*,*O*,*P*)-Xantphos ligands on each metal center with a facial coordination geometry, i.e., [Ir(κ^3(*P*,*O*,*P*)-Xantphos)(H)(μ-H)]$_2$[BAr′$_4$]$_2$ [20]. The Ir–Si1 and Ir–Si2 distances (2.3160(15) and 2.3171(16) Å, respectively) are typical of Ir–Si single bonds. The two largest bond angles around the iridium center are the P–Ir–O1 and Si2–Ir–O2 angles (176.09(10) and 154.65(11)°, respectively), indicating that Si1 is located at the apical position of the square pyramid.

The Ir–O2 bond (2.324(4) Å) is relatively long among common Ir–O(triflato) bonds (2.039(6)–2.401(12) Å) [8]. This is attributable to the large *trans* influence of a silyl ligand (Si2) located *trans* to the triflato ligand. A similar trend for a triflato ligand located *trans* to a silyl ligand has been observed in the iridium complex with a bis(2-pyridyloxy)methylsilyl (NSiN) ligand Ir(H)(coe)(OTf)(NSiN) where the Ir–O(triflato) distance is 2.36 Å (the averaged value for two crystallographically independent molecules) [1l].

The Ir···C22(γ-position of PCy_3) interatomic distance (3.123(6) Å) implies the existence of one γ-C–H agostic interaction at the position *trans* to apical Si1 on iridium. This distance is close to the sum of the van der Waals radius of a methylene group [14] and a single-bond covalent radius of iridium (1.22 Å) [15], and is slightly shorter than the corresponding Ir···C$_\gamma$(agostic) distances for **1a** (3.192(5) and 3.390(5) Å). The IR spectrum of **3** exhibits a weak absorption band attributable to the C–H stretching vibration of the agostic interaction at 2721 cm^{-1}, which lies at nearly the highest wavenumber region for ν_{CH} in various C–H agostic interactions (2250–2800 cm^{-1}) [21]. Analogous to the strength of the agostic interactions in **1a** (vide supra), the long Ir···C22 interatomic distance for **3** also indicates that this interaction is substantially weak. Thus, complex **3** can be regarded as a 16-electron complex.

The ^{1}H NMR spectrum of **3** in CD_2Cl_2 shows two singlets assigned to the SiMe protons at 0.34 and 0.76 ppm. The ^{29}Si{^{1}H} NMR spectrum of **3** in CD_2Cl_2 exhibits a doublet at −9.4 ppm ($^2J_{SiP}$ = 9.6 Hz). These data clearly shows that two silicon atoms in **3** are equivalent and that two methyl groups on the same silicon atom are inequivalent. Nevertheless, in the crystal structure shown in Fig. 4, two silicon atoms are inequivalent. Therefore, there must be a dynamic process involving exchange of the two silicon moieties in solution. A plausible process is the site change of the triflato ligand.

The IR spectrum of **3** shows an absorption band at 1317 cm^{-1} assignable to the $\nu_{S=O}$ stretching vibration of the coordinated triflato ligand. This wavenumber is close to that for (η^5-C_5Me_5)Ir(P-Me$_3$)(OTf)$_2$ (1324 cm^{-1}) in which the OTf groups are coordinated to the iridium atom [22].

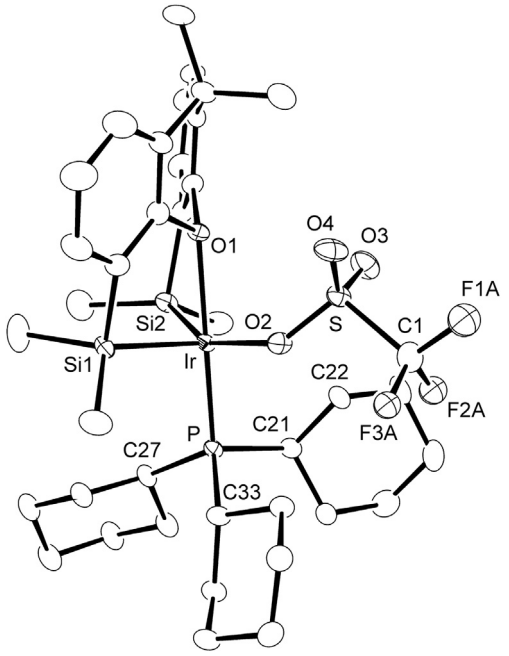

Fig. 4. Molecular structure of Ir{κ^3(*Si*,*O*,*Si*)-xantsil}(PCy_3)(OTf) (**3**) (50% probability ellipsoids). Hydrogen atoms are omitted for clarity. Each of the three fluorine atoms of the triflato ligand is disordered over two sites with the occupancy factors 0.51:0.49. Each one of the disordered atoms with the higher occupancy factor (F1A, F2A, and F3A) is depicted. Selected interatomic distances (Å) and angles (°) for **3**: Ir–P 2.2534(13), Ir–Si1 2.3160(15), Ir–Si2 2.3171(16), Ir–O1 2.245(4), Ir–O2 2.324(4), Ir···C22 3.123(6); P–Ir–Si1 101.41(5), P–Ir–Si2 93.97(5), P–Ir–O1 176.09(10), P–Ir–O2 102.72(10), Si1–Ir–Si2 100.77(6), Si1–Ir–O1 80.65(10), Si1–Ir–O2 94.53(11), Si2–Ir–O1 82.35(10), Si2–Ir–O2 154.65(11), O1–Ir–O2 80.33(13), Ir–P–C21 104.08(18), Ir–P–C27 116.97(19), Ir–P–C33 113.27(18), Ir–O2–S 127.8(2).

2.9. Estimation of the molecular structure of *1b* by comparison of NMR spectroscopic data for *1a*, *1b*, and *3*

The NMR data (^{1}H and ^{29}Si NMR chemical shifts, $^2J_{SiP}$ coupling constant) of the SiMe signals for triflato complex **3** are similar to those for chloro complex **1b** but are different from those for **1a**: The ^{1}H NMR chemical shifts (0.34 and 0.76 ppm) of the two SiMe signals for **3** in CD_2Cl_2 are almost identical with those for **1b** (0.36 and 0.77 ppm) but are fairly different from those for **1a** (0.72 and 0.85 ppm). Both the ^{29}Si NMR chemical shift and the $^2J_{SiP}$ coupling constant (−9.4 ppm, $^2J_{SiP}$ = 9.6 Hz) for **3** are also much closer to the corresponding data for **1b** (−6.2 ppm, $^2J_{SiP}$ = 9.9 Hz) than those for **1a** (−17.5 ppm, $^2J_{SiP}$ = 8.4 Hz). Accordingly, it is highly probable that the molecular structure of **1b** is similar to that of **3**, i.e., a five-coordinate complex with a tridentate κ^3(*Si*,*O*,*Si*)-xantsil ligand (Schemes 2 and 3).

On the basis of this estimation and the discussions in 2.5 and 2.6, 14-electron κ^2(*Si*,*Si*)-xantsil complex **1a** is expected to be thermodynamically more stable than 16-electron κ^3(*Si*,*O*,*Si*)-xantsil complex **1b** both in the solid state and in solution. This feature of the iridium–xantsil complexes **1a** and **1b** contrasts with those of the previously known ruthenium, manganese, molybdenum, and tungsten κ^3(*Si*,*O*,*Si*)-xantsil complexes where the κ^3(*Si*,*O*,*Si*)-xantsil geometry exists exclusively both in the solid-state and in solution [5].

In contrast with the above feature of chloro complexes **1a** and **1b**, the exclusive formation of 16-electron (triflato)(κ^3(*Si*,*O*,*Si*)-xantsil) complex **3** in the reaction of **1a** + **1b** with AgOTf (Scheme 4) indicates that **3** is thermodynamically far more stable than the 14-electron triflato analog of **1a**, i.e., Ir{κ^2(*Si*,*Si*)-xantsil}(PCy_3)(OTf). This is mainly because the triflato ligand in **3**, which is less electron-donating than the chloro ligand in **1a** and **1b**, makes the metal

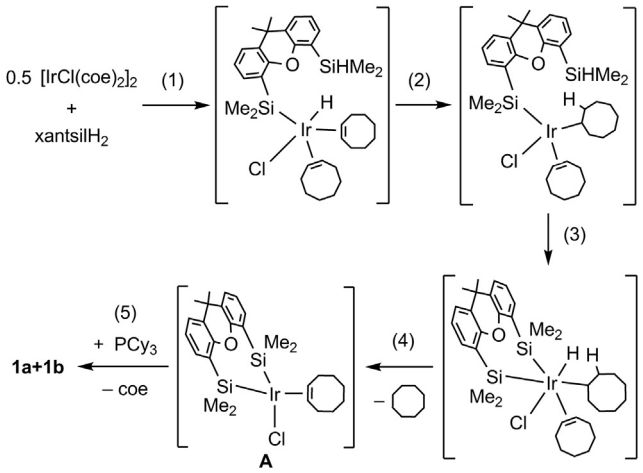

Scheme 5. A possible formation mechanism of **1a** + **1b** by the one-pot reaction of $[IrCl(coe)_2]_2$ with xantsilH_2 and then PCy_3.

center of **3** more electron deficient than those of **1a** and **1b** and, hence, strengthens the coordination of the xanthene oxygen to iridium in **3**.

*2.10. A possible formation mechanism of **1a** + **1b** by the one-pot synthesis from [IrCl(coe)$_2$]$_2$, xantsilH$_2$, and PCy$_3$*

A possible formation mechanism of iridium–xantsil complexes **1a** and **1b** by the reaction of $[IrCl(coe)_2]_2$ with xantsilH_2 and then PCy_3 in one-pot (Scheme 3, also see 2.3) is illustrated in Scheme 5. This mechanism involves (1) oxidative addition of one Si–H bond of xantsilH_2 to a coordinatively unsaturated $IrCl(coe)_2$ generated from the dimer $[IrCl(coe)_2]_2$, (2) migratory insertion of cyclooctene ligand into an Ir–H bond, (3) oxidative addition of the remaining Si–H bond of the xantsil(H) ligand, (4) C–H reductive elimination of cyclooctane to give an Ir–xantsil complex Ir(xantsil)(coe)Cl (**A**), and (5) replacement of the cyclooctene ligand in **A** by PCy_3.

*2.11. Reaction of complexes **1a** + **1b** with H$_2$*

When **1a** + **1b** was exposed to dihydrogen gas (1 atm) in C_6D_6 at room temperature, dihydrido complex **2** was formed in 51% NMR yield (95% conversion of **1a** + **1b**, conversion yield of **2**: 54%) together with some minor products (Scheme 2). This result and the previously mentioned result in the reaction of **2** with 3,3-dimethylbut-1-ene demonstrate that complexes **1a** + **1b** and **2** are interconvertible via oxidative addition of dihydrogen (from **1a** + **1b** to **2**) and alkene hydrogenation (from **2** to **1a** + **1b**).

*2.12. Hydrogenation of 3,3-dimethylbut-1-ene catalyzed by Ir–xantsil complexes **1a** + **1b** and **2***

According to the above-mentioned finding, it is expected that complexes **1a** + **1b** and **2** are catalytically active for alkene hydrogenation. Thus, by employing **1a** + **1b** and **2** as catalysts, we examined the hydrogenation of 3,3-dimethylbut-1-ene (Scheme 6). In the presence of 5 mol% of **1a** + **1b**, 3,3-dimethylbut-1-ene was exposed to dihydrogen (1 atm) in C_6D_6. The reaction completed in 32 h at 40 °C to give 2,2-dimethylbutane in 95% NMR yield (100% conversion of the alkene, TON = 19). Complex **2** (5 mol%) also promoted the same reaction under similar conditions to produce 2,2-dimethylbutane in 87% NMR yield. Thus, in the hydrogenation reaction catalyzed by **1a** + **1b**, the initial step is probably the

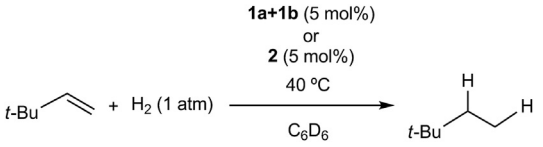

Scheme 6. Catalytic hydrogenation of 3,3-dimethylbut-1-ene promoted by **1a** + **1b** or **2**.

formation of dihydrido complex **2** by the oxidative addition of H_2. High yields of the alkane in these reactions indicate that the xantsil complexes serve as active catalysts for this hydrogenation.

3. Conclusions

In conclusion, we newly synthesized and characterized a 14-electron four-coordinate iridium(III) complex **1a** bearing a bidentate κ^2(*Si*,*Si*)-xantsil ligand. Complex **1a** adopts a distorted seesaw-shaped geometry due to the existence of two γ-C–H agostic interactions that are considerably weakened by strong *trans*-influence of two silyl ligands located at the positions *trans* to the γ-C–H bonds. Complex **1a** was also found to be in equilibrium with a smaller amount of its isomer, 16-electron κ^3(*Si*,*O*,*Si*)-xantsil complex **1b**, in solution, whereas **1a** exists exclusively in the crystals formed from the solution. Chloride substitution reaction of **1a** + **1b** with AgOTf gave quantitatively a single 16-electron triflato complex **3** having a tridentate κ^3(*Si*,*O*,*Si*)-xantsil ligand. The molecular structure of **1b** was estimated by comparing the NMR spectroscopic data with those for **3**.

1a + **1b** and 16-electron (dihydrido)iridium complex **2** are interconvertible: Oxidative addition of dihydrogen to **1a** + **1b** afforded **2**, while treatment of **2** with 3,3-dimethylbut-1-ene, a hydrogen acceptor, regenerated **1a** + **1b**. Applying these findings, we found that both **1a** + **1b** and **2** function as catalysts for hydrogenation of 3,3-dimethylbut-1-ene.

This study demonstrates that the xantsil ligand is a useful supporting ligand that effectively stabilizes a coordinatively unsaturated iridium center. We are expecting that iridium–xantsil complexes **1**–**3** can serve as active catalysts for various transformation reactions other than olefin hydrogenation. Further studies on reactions of **1**–**3** with organic and inorganic molecules and their application to catalytic reactions are in progress.

4. Experimental section

4.1. General procedures

All manipulations were carried out under dry argon in a glovebox or using a standard high-vacuum line and Schlenk techniques.

4.1.1. Materials

Benzene-d_6, toluene, toluene-d_8, hexane, and CH_2Cl_2 were dried over CaH_2 and vacuum transferred. All solvents were stored under argon over 4 Å molecular sieves in a glovebox. Tricyclohexylphosphine (PCy_3) (Strem Chemicals) was used as received. $[IrCl(coe)_2]_2$ [23] and 4,5-bis(dimethylsilyl)-9,9-dimethylxanthene (xantsilH_2) [5a,b] were prepared according to the literature methods.

4.1.2. Spectroscopic measurements

^1H, $^{13}C\{^1H\}$, $^{29}Si\{^1H\}$, and $^{31}P\{^1H\}$ NMR spectra in solution were recorded on a Bruker AVANCE III 400, a JEOL JNM-ECA 600, or a JEOL JNM-ECA 700 Fourier transform spectrometer. $^{29}Si\{^1H\}$ NMR measurements were performed using the DEPT pulse sequence or

using an inverse gate decoupling (IG) pulse sequence. The residual proton (C_6D_5H, 7.15 ppm; $C_6D_5CD_2H$, 2.09 ppm; $CDHCl_2$, 5.32 ppm) and the carbon resonances (C_6D_6, 128.0 ppm; CD_2Cl_2, 53.8 ppm) of deuterated solvents were used as internal references for ^1H and ^{13}C NMR chemical shifts, respectively. Aromatic protons or carbons are abbreviated as ArH and ArC, respectively. $^{29}Si\{^1H\}$ NMR chemical shifts were referenced to $SiMe_4$ (0 ppm) as an external standard. The NMR data were collected at room temperature unless indicated otherwise. 2D exchange spectroscopy (EXSY) measurements were carried out using a standard pulse sequence for phase-sensitive $^1H-^1H$ NOESY spectra [10]. The solid-state $^{31}P\{^1H\}$ cross-polarization magic angle spinning (CPMAS) NMR spectrum of **1a** + **1b** was recorded on a JEOL JNM-ECA 800 Fourier transform spectrometer where the chemical shifts were referenced to $(NH_4)H_2PO_4$ (1.0 ppm) as an external standard. Infrared spectra were measured on a KBr pellet sample using a Horiba FT-720 spectrometer. Mass spectra and high-resolution mass spectra (HRMS) were recorded on a Bruker Daltonics solariX 9.4T spectrometer operating in the electrospray ionization (ESI) mode or on a JEOL JMS-T100GCV spectrometer operating in the field desorption (FD) mode. Elemental analyses were carried out using a J-Science Lab JM11 microanalyzer. Measurements of mass spectra and elemental analyses were performed at the Research and Analytical Center for Giant Molecules, Tohoku University.

4.2. Synthesis of Ir{κ^2(*Si*,*Si*)-xantsil}(H)$_2$(PCy$_3$)Cl (**2**)

$[IrCl(coe)_2]_2$ (0.143 g, 0.160 mmol), xantsilH_2 (0.112 g, 0.343 mmol), and PCy_3 (0.123 g, 0.439 mmol) were dissolved in toluene (5 mL), and then the solution was stirred at room temperature for 1 h. The resulting red solution was evaporated to dryness under vacuum. The residue was washed with hexane (ca. 1 mL × 3) and dried under vacuum. Complex **2** was obtained as a pale-yellow powder in 68% yield (0.181 g, 0.217 mmol). ^1H NMR (400 MHz, C_6D_6): δ −14.33 (br s, $\Delta\nu_{1/2}$ = 117 Hz, 1H, Ir−H), −5.34 (br d, $^2J_{HP}$ = 99 Hz, 1H, Ir−H), 0.52–0.70 (m, 3H, PCy_3), 0.70–0.89 (m, 6H, PCy_3), 0.86 (s, 6H, SiMe), 0.97–1.14 (m, 6H, PCy_3), 1.18 (d, 6H, $^3J_{HP}$ = 1.2 Hz, SiMe), 1.33–1.50 (m, 9H, PCy_3), 1.37 (s, 3H, 9-CMe), 1.55 (s, 3H, 9-CMe), 1.65–1.81 (m, 6H, PCy_3), 1.92–2.06 (m, 3H, PCy_3), 6.95 (t, 2H, $^3J_{HH}$ = 7.3 Hz, ArH), 7.13–7.17 (m, 2H, ArH), 7.19 (dd, 2H, $^3J_{HH}$ = 7.3 Hz, $^4J_{HH}$ = 1.4 Hz, ArH). An ArH signal at δ 7.13–7.17 was partially overlapped with the residual proton signal of C_6D_6. ^1H NMR (600 MHz, 243 K, $C_6D_5CD_3$): δ −14.16 (d, $^2J_{HP}$ = 22 Hz, 1H, Ir−H), −5.07 (d, $^2J_{HP}$ = 112 Hz, 1H, Ir−H), 0.52–0.66 (m, 3H, PCy_3), 0.66–0.81 (m, 6H, PCy_3), 0.85 (s, 6H, SiMe), 1.01–1.16 (m, 6H, PCy_3), 1.20 (br s, 6H, $\Delta\nu_{1/2}$ = 3.2 Hz, SiMe), 1.38–1.53 (m, 9H, PCy_3), 1.36 (s, 3H, 9-CMe), 1.53 (s, 3H, 9-CMe), 1.60–1.80 (m, 6H, PCy_3), 1.91–2.04 (m, 3H, PCy_3), 6.95 (t, 2H, $^3J_{HH}$ = 7.2 Hz, ArH), 7.10–7.14 (m, 2H, ArH), 7.16 (dd, 2H, $^3J_{HH}$ = 7.2 Hz, $^4J_{HH}$ = 1.4 Hz, ArH). An ArH signal at δ 7.10–7.14 was partially overlapped with a residual ArH signal of $C_6D_5CD_3$. $^{13}C\{^1H\}$ NMR (101 MHz, C_6D_6): δ 2.7 (s with satellites, $^1J_{SiC}$ = 47 Hz, SiMe), 12.1 (d, $^3J_{CP}$ = 7.5 Hz, SiMe), 22.7 (9-C*Me*), 26.0 (PCy_3), 27.4 (d, $^2J_{CP}$ = 10 Hz, PCy_3), 29.3 (PCy_3), 30.8 (9-C*Me*), 33.2 (d, $^1J_{CP}$ = 20 Hz, PCy_3), 36.7 (9-*C*Me), 123.2, 125.2, 129.8, 135.2, 135.3, 158.6 (ArC). $^{29}Si\{^1H\}$ NMR (79.5 MHz, DEPT, C_6D_6): δ −1.6. $^{31}P\{^1H\}$ NMR (162 MHz, C_6D_6): δ 41.5. IR (KBr-pellet): 3053 (w, ν_{CH}), 2925 (s, ν_{CH}), 2850 (m, ν_{CH}), 2297 (w, ν_{IrH}), 2173 (w, ν_{IrH}), 1603 (w), 1444 (w), 1392 (s), 1244 (w), 1232 (w), 1215 (s), 1194 (w), 1124 (w), 1005 (w), 876 (w), 841 (m), 823 (s), 816 (s), 798 (m), 775 (s), 754 (s), 673 (w), 638 (m), 511 (w), 445 (m) cm^{-1}. HRMS (ESI, acetone solution): *m*/*z* calcd for $[C_{37}H_{59}OSi_2PClIr + Na]^+$ 857.3052, found 857.3048. NaI was added to the sample. Anal. Calcd for $C_{37}H_{59}OSi_2PClIr$: C, 53.24; H, 7.12. Found: C, 53.59; H, 7.00.

4.3. Synthesis of Ir(xantsil)(PCy$_3$)Cl (**1a** + **1b**)

Method A: A toluene (5 mL) solution of 3,3-dimethylbut-1-ene (0.024 g, 0.29 mmol) was added to complex **2** (0.105 g, 0.126 mmol). The solution was stirred at 60 °C for 30 h. The reaction mixture was filtered through a membrane filter (Nihon Millipore, Omnipore membrane, pore size 0.2 μm, 25 mm in diameter). After the filtrate was concentrated under vacuum, hexane was added to the concentrated solution, and then the solution was stored overnight at −35 °C in a freezer. A reddish orange solid was precipitated in the solution. The mother liquor was removed, and the solid was washed with hexane and was dried under vacuum. Ir{κ^2(*Si*,*Si*)-xantsil}(PCy_3)Cl (**1a**) (0.047 g, 0.056 mmol) was obtained as a reddish orange powder in 45% yield. The product exists as a 5:1 equilibrium mixture of isomeric complexes **1a** and **1b** in CD_2Cl_2 but exists as only **1a** in the solid state.

*Method B (One-pot synthesis of **1a** + **1b** from [IrCl(coe)$_2$]$_2$)*: In a Schlenk tube, $[IrCl(coe)_2]_2$ (0.144 g, 0.161 mmol) and xantsilH_2 (0.123 g, 0.377 mmol) were dissolved in toluene (5 mL). The solution was stirred at room temperature for 30 min. To the resulting mixture was added PCy_3 (0.106 g, 0.378 mmol), and then the mixture was stirred at room temperature for further 30 min. The brown reaction mixture was filtered through a Whatman PTFE syringe filter (pore size: 0.45 μm), and the filtrate was concentrated under vacuum until most of volatiles were evaporated. When hexane was added to the concentrated solution, a reddish orange solid was precipitated. The solution containing the solid was cooled to −35 °C overnight. Removing the mother liquor, washing the solid with hexane, and drying under vacuum gave **1a**(+**1b**) (0.128 g, 0.154 mmol, 48%) as a reddish orange powder. Data for **1a**: ^1H NMR (400 MHz, C_6D_6): δ ca. 0.6–1.8 (m, 33H, PCy_3), 0.93 (s, 6H, SiMe), 1.40 (s, 3H, 9-CMe), 1.45 (s, 6H, SiMe), 1.56 (s, 3H, 9-CMe), 6.96 (t, 2H, $^3J_{HH}$ = 7.3 Hz, ArH), 7.13–7.18 (m, 2H, ArH), 7.25 (dd, 2H, $^3J_{HH}$ = 7.3 Hz, $^4J_{HH}$ = 1.4 Hz, ArH). The chemical shifts of the signals of PCy_3 could not be determined exactly due to the overlap with those of **1b**. An ArH signal at δ 7.13–7.18 was partially overlapped with the residual proton signal of C_6D_6. ^1H NMR (400 MHz, CD_2Cl_2): δ 0.72 (s, 6H, SiMe), ca. 0.8–2.0 (m, 33H, PCy_3), 0.85 (s, 6H, SiMe), 1.46 (s, 3H, 9-CMe), 1.80 (s, 3H, 9-CMe), 7.05 (t, 2H, $^3J_{HH}$ = 7.4 Hz, ArH), 7.21 (dd, 2H, $^3J_{HH}$ = 7.4 Hz, $^4J_{HH}$ = 1.4 Hz, ArH), 7.37 (dd, 2H, $^3J_{HH}$ = 7.4 Hz, $^4J_{HH}$ = 1.4 Hz, ArH). The chemical shifts of the signals of PCy_3 could not be determined exactly due to the overlap with those of **1b**. $^{13}C\{^1H\}$ NMR (101 MHz, CD_2Cl_2): δ 2.1 (SiMe), 8.2 (SiMe), 22.6 (9-C*Me*), 26.3 (PCy_3), 28.1 (d, $^2J_{CP}$ = 10.2 Hz, PCy_3), 29.8–31.8 (br, PCy_3), 30.7 (9-C*Me*), 37.1 (9-*C*Me), 37.8–39.1 (br, PCy_3), 123.7, 125.6, 129.9, 132.5 (d, $^3J_{CP}$ = 2.5 Hz), 135.2, 159.4 (ArC). Assignments of the ^1H and ^{13}C signals were confirmed by $^1H-^{13}C$ HSQC and $^1H-^{13}C$ HMBC NMR spectra. $^{29}Si\{^1H\}$ NMR (79.5 MHz, IG, CD_2Cl_2): δ −17.5 (d, $^2J_{SiP}$ = 8.4 Hz). $^{31}P\{^1H\}$ NMR (162 MHz, C_6D_6): δ 1.8 (br s, $\Delta\nu_{1/2}$ = 12 Hz). $^{31}P\{^1H\}$ NMR (162 MHz, CD_2Cl_2): δ 0.5 (br s, $\Delta\nu_{1/2}$ = 12 Hz). $^{31}P\{^1H\}$ CPMAS NMR (324 MHz, spinning rate: 22 kHz): δ −2.1, 1.1. Data for **1b**: ^1H NMR (400 MHz, C_6D_6): δ 0.53 (s, 6H, SiMe), 1.00 (s, 6H, SiMe), 2.12–2.28 (m, 6H, PCy_3), 2.35–2.53 (m, 3H, PCy_3), 7.05–7.09 (m, 4H, ArH), 7.36–7.41 (m, 2H, ArH). The 9-CMe signals of the xanthene backbone and other ^1H signals of PCy_3 could not be assigned because of the overlap with ^1H signals of **1a**. ^1H NMR (400 MHz, CD_2Cl_2): δ 0.36 (s, 6H, SiMe), 0.77 (s, 6H, SiMe), ca. 0.8–2.0 (m, 24H, PCy_3), 1.60 (s, 3H, 9-CMe), 1.82 (s, 3H, 9-CMe), 2.08–2.26 (m, 6H, PCy_3), 2.32–2.49 (m, 3H, PCy_3), 7.15 (t, 2H, $^3J_{HH}$ = 7.3 Hz, ArH), 7.29–7.35 (m, 4H, ArH). The chemical shifts of the signals of PCy_3 at δ ca. 0.8–2.0 could not be determined exactly due to the overlap with those of **1a**. $^{13}C\{^1H\}$ NMR (101 MHz, CD_2Cl_2): δ 5.5 (SiMe), 8.0 (SiMe), 22.7 (9-C*Me*), 30.2 (9-C*Me*), 37.6 (9-*C*Me), 123.4, 124.6, 129.7, 133.1, 136.1, 160.2 (ArC). The signals of PCy_3 could not be assigned due to the overlap with those of **1a** and

unidentified impurities. Assignments of the ^{1}H and ^{13}C signals were confirmed by $^{1}H-^{13}C$ HSQC and $^{1}H-^{13}C$ HMBC NMR spectra. $^{29}Si\{^{1}H\}$ NMR (79.5 MHz, IG, CD_2Cl_2): δ −6.2 (d, $^{2}J_{SiP}$ = 9.9 Hz). $^{31}P\{^{1}H\}$ NMR (162 MHz, C_6D_6): δ 9.6 (br s, $\Delta\nu_{1/2}$ = 7 Hz). $^{31}P\{^{1}H\}$ NMR (162 MHz, CD_2Cl_2): δ 9.1 (br s, $\Delta\nu_{1/2}$ = 8 Hz). Data for a solid sample of **1a**(+**1b**): IR (KBr-pellet): 3053 (w, ν_{CH}), 2929 (s, ν_{CH}), 2852 (s, ν_{CH}), 2819 (m, ν_{CH}), 1604 (w), 1446 (m), 1427 (w), 1392 (s), 1267 (w), 1234 (m), 1219 (s), 1192 (m), 1174 (w), 1122 (m), 1003 (w), 877 (w), 835 (s), 816 (s), 793 (s), 773 (s), 750 (s), 735 (s), 673 (w), 638 (m), 513 (w), 447 (m), 424 (w), 407 (m) cm^{-1}. HRMS (FD): *m*/*z* calcd for $[C_{37}H_{57}OSi_2PClIr]^{+}$ 832.2998, found 832.3013. Anal. Calcd for $C_{37}H_{57}OSi_2PClIr$: C, 53.37; H, 6.90. Found: C, 53.34; H, 6.93.

4.4. Reaction of Ir(xantsil)(PCy_3)Cl (**1a** + **1b**) with AgOTf: synthesis of Ir{κ^3(*Si,O,Si*)-xantsil}(PCy_3)(OTf) (**3**)

To **1a** + **1b** (0.047 g, 0.056 mmol) in a Schlenk tube was added a suspension of AgOTf (0.014 g, 0.054 mmol) in toluene (2 mL). The tube was covered with a piece of aluminum foil to shield the sample against the light, and the mixture was stirred at room temperature for 20 min. The reaction mixture was filtered through a membrane filter (Nihon Millipore, Omnipore membrane, pore size 0.2 μm, 25 mm in diameter). The yellow filtrate was concentrated under vacuum. A yellow solid was precipitated in the solution. Hexane was added to the solution containing the solid, and then the suspension was stored at −35 °C in a freezer for 1 h. The solid was collected by filtration through a membrane filter and was dried under vacuum. Ir{κ^3(*Si,O,Si*)-xantsil}(PCy_3)(OTf) (**3**)·0.5toluene (0.035 g, 0.035 mmol) was obtained as a yellow powder in 65% yield based on AgOTf. ^{1}H NMR (400 MHz, C_6D_6): δ 0.31 (s, 6H, SiMe), 0.50–2.90 (m, 33H, PCy_3), 0.83 (s, 6H, SiMe), 1.43 (s, 3H, 9-CMe), 1.92 (s, 3H, 9-CMe), 7.05 (t, 2H, $^{3}J_{HH}$ = 7.3 Hz, ArH), 7.11 (dd, 2H, $^{3}J_{HH}$ = 7.3 Hz, $^{4}J_{HH}$ = 1.2 Hz, ArH), 7.27 (dd, 2H, $^{3}J_{HH}$ = 7.3 Hz, $^{4}J_{HH}$ = 1.2 Hz, ArH). ^{1}H NMR (400 MHz, CD_2Cl_2): δ 0.34 (s, 6H, SiMe), 0.76 (s, 6H, SiMe), 1.15–1.45 (m, 9H, PCy_3), 1.67 (s, 3H, 9-CMe), 1.71–2.05 (br, 15H, PCy_3), 1.82 (s, 3H, 9-CMe), 2.06–2.29 (br, 6H, PCy_3), 2.38–2.72 (br, 3H, PCy_3), 7.21 (t, 2H, $^{3}J_{HH}$ = 7.3 Hz, ArH), 7.32 (dd, 2H, $^{3}J_{HH}$ = 7.3 Hz, $^{4}J_{HH}$ = 1.1 Hz, ArH), 7.42 (dd, 2H, $^{3}J_{HH}$ = 7.3 Hz, $^{4}J_{HH}$ = 1.1 Hz, ArH). $^{13}C\{^{1}H\}$ NMR (101 MHz, CD_2Cl_2): δ 2.7 (s with satellites, $^{1}J_{SiC}$ = 46 Hz, SiMe), 6.0 (s with satellites, $^{1}J_{SiC}$ = 49 Hz, SiMe), 24.0 (9-C*Me*), 26.6 (PCy_3), 27.9 (d, $^{2}J_{CP}$ = 10.7 Hz, PCy_3), 28.7–34.5 (br, $\Delta\nu_{1/2}$ = 134 Hz, PCy_3), 30.9 (9-C*Me*), 37.7 (9-CMe), 38.5–44.6 (br, $\Delta\nu_{1/2}$ = 202 Hz, PCy_3), 120.7 (q, $^{1}J_{CF}$ = 320.6 Hz, CF_3), 125.9, 126.1, 129.3, 129.5, 136.5, 160.7 (ArC). Assignments of the ^{1}H and ^{13}C signals were confirmed by $^{1}H-^{13}C$ HSQC and $^{1}H-^{13}C$ HMBC NMR spectra. $^{29}Si\{^{1}H\}$ NMR (79.5 MHz, DEPT, C_6D_6): δ −9.5 (d, $^{2}J_{SiP}$ = 9.7 Hz). $^{29}Si\{^{1}H\}$ NMR (79.5 MHz, DEPT, CD_2Cl_2): δ −9.4 (d, $^{2}J_{SiP}$ = 9.6 Hz). $^{31}P\{^{1}H\}$ NMR (162 MHz, C_6D_6): δ 1.0. $^{31}P\{^{1}H\}$ NMR (162 MHz, CD_2Cl_2): δ 1.6. IR (KBr-pellet): 3043 (w, ν_{CH}), 2931 (m, ν_{CH}), 2852 (m, ν_{CH}), 2721 (w, ν_{CH}), 1448 (w), 1421 (w), 1389 (s), 1317 (s, $\nu_{S=O}$), 1230 (s), 1207 (s), 1201 (s), 1159 (m), 1144 (m), 1115 (w), 1086 (w), 1024 (m), 1011 (s), 839 (m), 823 (m), 802 (m), 785 (m), 764 (m), 731 (w), 675 (w), 648 (w), 633 (s), 540 (w), 517 (w), 444 (w), 409 (w) cm^{-1}. FD-MS: *m*/*z* 946 (M^{+}, 10), 797 (M^{+} − OTf, 100). Anal. Calcd for $C_{38}H_{57}O_4F_3Si_2PSIr$ + 0.5 C_7H_8: C, 50.23; H, 6.20. Found: C, 49.89; H, 6.07.

4.5. NMR monitoring of a reaction of Ir(xantsil)(PCy_3)Cl (**1a** + **1b**) with dihydrogen

1a + **1b** (6 mg, 7 μmol) and Cp_2Fe (internal standard, less than 1 mg; Cp = η^5-C_5H_5) were dissolved in C_6D_6 (0.6 mL). The solution was transferred to an NMR tube with a J-Young Teflon valve (5 mm o.d.). A ^{1}H NMR spectrum of the mixture was measured to determine the ratio of the intensities of signals of **1a**, **1b**, and Cp_2Fe. The NMR tube was evacuated briefly to degas, and 1 atm of H_2 was then applied to the tube. This procedure was repeated three times, and then the tube was shaken well. Conversion of **1a** and **1b** at room temperature was monitored by ^{1}H NMR spectroscopy. Dihydrido complex **2** was formed as the main product. The maximum NMR yield of **2** (51%) was attained after 24 h (95% conversion of **1a** + **1b**, conversion yield of **2**: 54%). The NMR yield was determined by comparison of the intensities of the SiMe signals for **1a**, **1b**, and **2** with that of the Cp_2Fe signal. The product **2** was identified by comparing the ^{1}H and $^{31}P\{^{1}H\}$ NMR spectra with those of the sample synthesized by the procedure described in section 4.2. Prolonged exposure of the reaction mixture to H_2 resulted in decrease of **2** and formation of unidentified products.

4.6. NMR monitoring of a reaction of 3,3-dimethylbut-1-ene with dihydrogen catalyzed by Ir(xantsil)(PCy_3)Cl (**1a** + **1b**)

1a + **1b** (5 mg, 6 μmol), 3,3-dimethylbut-1-ene (11 mg, 0.13 mmol), and Cp_2Fe (internal standard, less than 1 mg) were dissolved in C_6D_6 (0.6 mL). The solution was transferred to an NMR tube with a J-Young Teflon valve (5 mm o.d.). A ^{1}H NMR spectrum of the mixture was measured to determine the ratio of the intensities of the signals of 3,3-dimethylbut-1-ene and the signal of Cp_2Fe. The NMR tube was evacuated briefly to degas, and then charged with 1 atm of H_2 gas. This procedure was repeated three times. The tube was shaken well and then heated at 40 °C, and the conversion of 3,3-dimethylbut-1-ene was monitored by ^{1}H NMR spectroscopy. After heating for 32 h, the alkene was completely consumed and 2,2-dimethylbutane was formed in 95% NMR yield (100% conversion of the alkene, TON = 19). During the reaction, the tube was shaken well after 1, 5, 7, and 24 h to dissolve dihydrogen gas and volatile 3,3-dimethylbut-1-ene (b.p. 41 °C) in the solution, and after 20 h of the reaction the tube was charged again with 1 atm of H_2 gas. The product (2,2-dimethylbutane) was identified by comparing the ^{1}H and $^{13}C\{^{1}H\}$ NMR spectra and the retention time of gas chromatography (column: SE-30 packed column, carrier gas: N_2, detector: FID) with those of the authentic sample.

4.7. NMR monitoring of a reaction of 3,3-dimethylbut-1-ene with dihydrogen catalyzed by Ir{κ^2(*Si,Si*)-xantsil}$(H)_2$(PCy_3)Cl (**2**)

The title reaction was monitored by a procedure similar to that for the above-mentioned hydrogenation catalyzed by **1a** + **1b** using **2** (5 mg, 6 μmol), 3,3-dimethylbut-1-ene (11 mg, 0.13 mmol), and Cp_2Fe (internal standard, less than 1 mg) in C_6D_6 (0.6 mL) at 40 °C. After 34 h, 2,2-dimethylbutane was formed in 87% NMR yield.

4.8. X-ray crystal structure determination

An X-ray quality single crystal of **2**·toluene (a pale-yellow plate) was obtained from a concentrated toluene solution at −35 °C in a freezer. That of **3**·0.2CH_2Cl_2 (a pale-yellow plate) was obtained from a hexane layered solution in CH_2Cl_2 at −35 °C. For **1a**·CH_2Cl_2, a reddish orange blocklike crystal for the X-ray analysis was selected from crystals obtained from a concentrated CH_2Cl_2 solution of **1a** + **1b** at −35 °C. Intensity data for the analysis were collected on a Rigaku RAXIS-RAPID imaging plate diffractometer with graphite-monochromated Mo Kα radiation (λ = 0.71069 Å) under a cold nitrogen stream (T = 150 K). Numerical absorption corrections were applied to the data. The structures were solved by the Patterson method using the DIRDIF-2008 program [24] and refined by full matrix least-squares techniques on all F^2 data with SHELXL-97 [25]. Each of the three fluorine atoms of the triflato ligand in **3** was disordered over two sites with the occupancy factors 0.51:0.49. These atoms were refined isotropically. In the case of **1a**·CH_2Cl_2, each of the two chlorine atoms of a CH_2Cl_2 molecule, the solvent of

crystallization, was disordered over two sites with the occupancy factors 0.67:0.33. For **3**·0.2CH_2Cl_2, the structure refinement was carried out by assuming partial occupancy (occupancy factor = 0.20) of the solvent of crystallization (CH_2Cl_2) because the determined electron density of the CH_2Cl_2 was far less than expected for one molecule. The carbon and chlorine atoms of the solvent molecules in **1a**·CH_2Cl_2 and **3**·0.2CH_2Cl_2 were refined isotropically, and no hydrogen atoms on the carbon atoms were included. Except for these solvent molecules and the disordered atoms, anisotropic refinements were applied to all non-hydrogen atoms. Two hydrido hydrogen atoms of **2** were not located in the difference Fourier map and were not included in the refinement. Other hydrogen atoms were placed at calculated positions. The correct absolute structure of **1a** was confirmed by refinement of the Flack parameter (0.000(4)) [26]. All calculations were carried out using Yadokari-XG 2009 [27]. Selected crystallographic data for **1a**, **2**, and **3** are listed in Table B1 (see the Supplementary material).

Acknowledgments

This work was supported by Grants-in-Aid for Scientific Research (Grant Numbers 25410058, 22350024, and 23750053) from the Japan Society for the Promotion of Science (JSPS) and also partly supported by "Nanotechnology Platform" of the Ministry of Education, Culture, Sports, Science and Technology (MEXT), Japan, at the Center for Integrated Nanotechnology Support, Tohoku University. We are grateful to Mr. Shinichiro Yoshida (Tohoku University) for his help with the 2D EXSY measurements of **1a** + **1b** and **2** and with the solid-state NMR spectroscopic measurements of **1a** + **1b**. We also acknowledge the Research and Analytical Center for Giant Molecules, Tohoku University, for spectroscopic measurements and elemental analyses. This work was also performed under the Cooperative Research Program of "Network Joint Research Center for Materials and Devices". We acknowledge Prof. Hideo Nagashima (Kyusyu University) for his warm support in this program. We are also grateful to Ms. Keiko Ideta for her help with the low-temperature NMR spectroscopic measurements of **2** and with the determination of spin-lattice relaxation times (T_1) of **2** in the Evaluation Center of Materials Properties and Function, Institute for Material Chemistry and Engineering, Kyusyu University.

Appendix A. Supplementary material

CCDC 959048, 959049, and 959050 contain the supplementary crystallographic data for this paper. These data can be obtained free of charge from The Cambridge Crystallographic Data Centre via www.ccdc.cam.ac.uk/data_request/cif.

Appendix B. Supplementary data

Supplementary data related to this article can be found at http://dx.doi.org/10.1016/j.jorganchem.2013.09.009.

References

[1] For selected examples of iridium complexes bearing silyl-containing multidentate ligands, see: (a) M.J. Auburn, S.R. Stobart, Inorg. Chem. 24 (1985) 318; (b) P.I. Djurovich, A.L. Safir, N.L. Keder, R.J. Watts, Inorg. Chem. 31 (1992) 3195; (c) M.J. Auburn, R.D. Holmes-Smith, S.R. Stobart, P.K. Bakshi, T.S. Cameron, Organometallics 15 (1996) 3032; (d) M. Okazaki, H. Tobita, H. Ogino, J. Chem. Soc. Dalton Trans. (1997) 3531; (e) M. Stradiotto, K.L. Fujdala, T.D. Tilley, Chem. Commun. (2001) 1200; (f) P. Sangtrirutnugul, T.D. Tilley, Organometallics 26 (2007) 5557; (g) D.F. MacLean, R. McDonald, M.J. Ferguson, A.J. Caddell, L. Turculet, Chem. Commun. (2008) 5146; (h) E. Morgan, D.F. MacLean, R. McDonald, L. Turculet, J. Am. Chem. Soc. 131 (2009) 14234; (i) M.T. Whited, N.P. Mankad, Y. Lee, P.F. Oblad, J.C. Peters, Inorg. Chem. 48 (2009) 2507; (j) H. Fang, Y.-K. Choe, Y. Li, S. Shimada, Chem. Asian J. 6 (2011) 2512; (k) Y.-H. Li, Y. Zhang, X.-H. Ding, Inorg. Chem. Commun. 14 (2011) 1306; (l) R. Lalrempuia, M. Iglesias, V. Polo, P.J.S. Miguel, F.J. Fernández-Alvarez, J.J. Pérez-Torrente, L.A. Oro, Angew. Chem. Int. Ed. 51 (2012) 12824; (m) C.-I. Lee, J. Zhou, O.V. Ozerov, J. Am. Chem. Soc. 135 (2013) 3560.

[2] D.L. Lichtenberger, A. Rai-Chaudhuri, J. Am. Chem. Soc. 113 (1991) 2923.

[3] (a) J. Chatt, C. Eaborn, S. Ibekwe, Chem. Commun. (Lond.) (1966) 700; (b) J. Chatt, C. Eaborn, S.D. Ibekwe, P.N. Kapoor, J. Chem. Soc. A 125 (1970) 1343; (c) V.K. Dioumaev, L.J. Procopio, P.J. Carroll, D.H. Berry, J. Am. Chem. Soc. 125 (2003) 8043.

[4] M.C. MacInnis, R. McDonald, M.J. Ferguson, S. Tobisch, L. Turculet, J. Am. Chem. Soc. 133 (2011) 13622.

[5] (a) H. Tobita, K. Hasegawa, J.J.G. Minglana, L.-S. Luh, M. Okazaki, H. Ogino, Organometallics 18 (1999) 2058; (b) J.J.G. Minglana, M. Okazaki, K. Hasegawa, L.-S. Luh, N. Yamahira, T. Komuro, H. Ogino, H. Tobita, Organometallics 26 (2007) 5859; (c) J.J.G. Minglana, M. Okazaki, H. Tobita, H. Ogino, Chem. Lett. (2002) 406; (d) M. Okazaki, J.J.G. Minglana, N. Yamahira, H. Tobita, H. Ogino, Can. J. Chem. 81 (2003) 1350; (e) M. Okazaki, N. Yamahira, J.J.G. Minglana, H. Tobita, Organometallics 23 (2004) 4531; (f) M. Okazaki, N. Yamahira, J.J.G. Minglana, T. Komuro, H. Ogino, H. Tobita, Organometallics 27 (2008) 918; (g) H. Tobita, N. Yamahira, K. Ohta, T. Komuro, M. Okazaki, Pure Appl. Chem. 80 (2008) 1155; (h) R. Begum, T. Komuro, H. Tobita, Chem. Commun. (2006) 432; (i) R. Begum, T. Komuro, H. Tobita, Chem. Lett. 36 (2007) 650; (j) T. Komuro, R. Begum, R. Ono, H. Tobita, Dalton Trans. 40 (2011) 2348; (k) T. Komuro, S. Okawara, K. Furuyama, H. Tobita, Chem. Lett. 41 (2012) 774.

[6] (a) J.Y. Corey, Chem. Rev. 111 (2011) 863; (b) J.Y. Corey, J. Braddock-Wilking, Chem. Rev. 99 (1999) 175.

[7] For selected examples of iridium complexes having a bis(silyl) chelate ligand, see: (a) J. Greene, M.D. Curtis, J. Am. Chem. Soc. 99 (1977) 5176; (b) M. Loza, J.W. Faller, R.H. Crabtree, Inorg. Chem. 34 (1995) 2937; (c) Y.-J. Lee, J.-D. Lee, S.-J. Kim, J. Ko, I.-H. Suh, M. Cheong, S.O. Kang, Organometallics 23 (2004) 135; (d) H. Hashimoto, T. Suzuki, H. Tobita, Dalton Trans. 39 (2010) 9386.

[8] Based on a survey of the Cambridge Structural Database, CSD Version 5.34, November 2012.

[9] (a) D. Karshtedt, A.T. Bell, T.D. Tilley, Organometallics 25 (2006) 4471; (b) J.L. McBee, J. Escalada, T.D. Tilley, J. Am. Chem. Soc. 131 (2009) 12703.

[10] (a) C.L. Perrin, T.J. Dwyer, Chem. Rev. 90 (1990) 935; (b) L. Cronin, C.L. Higgitt, R.N. Perutz, Organometallics 19 (2000) 672.

[11] D.G. Hamilton, R.H. Crabtree, J. Am. Chem. Soc. 110 (1988) 4126.

[12] (a) R.H. Crabtree, C.P. Parnell, Organometallics 4 (1985) 519; (b) D.W. Lee, W.C. Kaska, C.M. Jensen, Organometallics 17 (1998) 1.

[13] The τ_4 value, developed by Houser et al. for evaluating the geometry of four-coordinate complexes, was calculated for **1a** as 0.75, which is close to the reported values (~0.70 ± 0.02) for complexes adopting a seesaw-shaped geometry. See: L. Yang, D.R. Powell, R.P. Houser Dalton Trans. (2007) 955.

[14] L. Pauling, The Nature of the Chemical Bond, third ed., Cornell University Press, Ithaca, New York, 1960, pp. 257–264.

[15] P. Pyykkö, M. Atsumi, Chem. Eur. J. 15 (2009) 186.

[16] (a) A.C. Cooper, E. Clot, J.C. Huffman, W.E. Streib, F. Maseras, O. Eisenstein, K.G. Caulton, J. Am. Chem. Soc. 121 (1999) 97; (b) A.C. Cooper, W.E. Streib, O. Eisenstein, K.G. Caulton, J. Am. Chem. Soc. 119 (1997) 9069.

[17] (a) N.M. Scott, R. Dorta, E.D. Stevens, A. Correa, L. Cavallo, S.P. Nolan, J. Am. Chem. Soc. 127 (2005) 3516; (b) R. Dorta, R. Goikhman, D. Milstein, Organometallics 22 (2003) 2806; (c) C.Y. Tang, N. Phillips, M.J. Kelly, S. Aldridge, Chem. Commun. 48 (2012) 11999.

[18] The solid sample used for the measurement of the $^{31}P\{^1H\}$ CPMAS NMR spectrum, which involves only **1a**, was dissolved in CD_2Cl_2, and the ^1H NMR spectrum of the solution was measured. The result revealed the formation of a mixture of **1a** and **1b** in 5:1 M ratio due to the fast equilibrium between them in solution.

[19] As a related phenomenon, Davies et al. reported that the plural signals (ca. 2:1 intensity ratio) were observed in the solid-state ^{31}P CPMAS NMR spectrum of tricyclohexylphosphine oxide ($OPCy_3$) due to the existence of three crystallographically independent molecules. See: J.A. Davies, S. Dutremez, A.A. Pinkerton Inorg. Chem. 30 (1991) 2380.

[20] A.J. Pontiggia, A.B. Chaplin, A.S. Weller, J. Organomet. Chem. 696 (2011) 2870.

[21] M. Brookhart, M.L.H. Green, L.-L. Wong, Prog. Inorg. Chem. 36 (1988) 1.

[22] P.J. Stang, Y.-H. Huang, A.M. Arif, Organometallics 11 (1992) 231.

[23] J.L. Herde, J.C. Lambert, C.V. Senoff, Inorg. Synth. 15 (1974) 18.

[24] P.T. Beurskens, G. Beurskens, R. de Gelder, S. Garcia-Granda, R.O. Gould, J.M.M. Smits, The DIRDIF2008 Program System, Crystallography Laboratory, University of Nijmegen, Nijmegen, The Netherlands, 2008.

[25] G.M. Sheldrick, Acta Crystallogr. Sect. A 64 (2008) 112.

[26] H.D. Flack, Acta Crystallogr. Sect. A 39 (1983) 876.

[27] (a) K. Wakita, Yadokari-XG, Software for Crystal Structure Analyses, 2001; (b) Yadokari-XG 2009, Software for Crystal Structure Analyses. See: C. Kabuto, S. Akine, T. Nemoto, E. Kwon J. Cryst. Soc. Jpn. 51 (2009) 218.